Orientation-dependent yield and Bauschinger effects in two-dimensional Yukawa solids

Shaoyu Lu,[1] Dong Huang,[1] Chen Liang,[1] and Yan Feng[1,2,*]

[1]*Institute of Plasma Physics and Technology, Jiangsu Key Laboratory of Frontier Material Physics and Devices, School of Physical Science and Technology, Soochow University, Suzhou 215006, China*

[2]*National Laboratory of Solid State Microstructures, Nanjing University, Nanjing 210093, China*

(Received 9 June 2024; accepted 12 August 2024; published 23 August 2024)

Langevin dynamics simulations of two-dimensional (2D) Yukawa solids are performed to investigate the orientation-dependent yield and Bauschinger effects in solid 2D dusty plasmas. The yield stress of 2D Yukawa solids under different conditions is determined from the corresponding stress-strain response curve, defect fraction, and deviation from the affine displacement. It is discovered that both the shear modulus and yield stress are orientation dependent, exhibiting the significant anisotropic behaviors. It is found that the dependence of the calculated atomic elastic constant on the lattice orientation completely agrees with those of the shear modulus and yield stress. It is also found that, for different initial lattice orientations, the Yukawa solid exhibits the significant regular or reverse Bauschinger effects, or even non-Bauschinger effect.

DOI: 10.1103/PhysRevResearch.6.033211

I. INTRODUCTION

For most solid materials beyond the elastic limit, a plastic deformation occurs and strains are not totally recoverable, which is termed as yield [1]. The stress that is necessary to initiate the plastic deformation is called the yield stress or yield point [1–3]. In crystal materials, the fundamental mechanism of the plastic deformation is believed to be the motion of dislocations [4,5], and the yield stress is the minimum stress at which the plastic deformation occurs for the studied material. In other words, the yield stress is equivalent to the critical stress under which the dislocation inside the material starts to move in the steady state [2]. Under an external loading, the dislocation would move along one of the slip systems [4], i.e., a preferred orientation of crystal planes and directions, so that an originally isotropic crystal may become anisotropic in many physical properties [6]. For example, the yield stress of the crystal material often exhibits significant anisotropic behaviors, like the Bauschinger effect [2,3,7].

The Bauschinger effect was first proposed for a steel material, which has a lower yield stress under the compressional loading after having been subject to a tension [7]. More generally, the Bauschinger effect is used to describe the lowering of the yield stress under the reverse loading following the previous forward loading [3]. The Bauschinger effect has been evidenced in most materials [8–15], such as single-crystal metals [8], polycrystalline metals [9], polymers [10], and amorphous materials [11]. When the deformation is loading history dependent, the Bauschinger effect plays an important role in the failure of materials, which has several important practical implications [8]. Therefore, understanding the fundamental origin of the Bauschinger effect is crucial in material processing and other related fields. For various materials or systems, quite a few theoretical models are proposed to interpret the origin of the Bauschinger effect, as in Refs. [8–11,13,16,17]. For example, the origin of the Bauschinger effect in metals is attributed to the back stress induced by the dislocation pileup [16]. In amorphous solids, the Bauschinger effect is associated with the anisotropic elasticity due to the deformation history [17], and the asymmetry distribution of the local residual strength [11]. In fact, until now, the origin of the Bauschinger effect is still a debated topic in various fields.

Dusty plasma, also termed as complex plasma, refers to a collection of μm-sized dust particles in the plasma environment [18–36]. In the typical laboratory conditions performed on the earth, tens of thousands dust particles are highly charged to $\sim -10^4 e$, forming a single-layer suspension in the plasma sheath, i.e., the two-dimensional (2D) dusty plasma [37–39]. Since these dust particles are highly charged, the potential energy between neighboring dust particles is much higher than their kinetic energy, so that these dust particles are strongly coupled, exhibiting the collective properties of liquids [40–45] or solids [46–53].

Based on the individual particle identification and tracking in experiments, dusty plasma is an excellent physical system to study various mechanical properties of solids at the individual particle level, including the elasticity [54–59] and plasticity [51–53]. Laser modulations are often used to apply external forces in 2D dusty plasma experiments to study the uniform melting [44,60], the shear deformation [52,53,61,62], the shear flows [63–65], and the shear-induced melting [66]. The yield stress of the solid 2D dusty plasma is also theoretically studied using numerical simulations [55], where the

*Contact author: fengyan@suda.edu.cn

shear force in two rectangular regions is applied to mimic the laser manipulation in experiments. However, in our literature search, we have not found any investigations of the orientation-dependent yield or the Bauschinger effect in dusty plasmas, as we study here. In addition to their underlying mechanisms, we also would like to investigate the relationship between the orientation-dependent yield and the Bauschinger effect in 2D solid dusty plasmas.

This paper is organized as follows. In Sec. II, we briefly introduce our Langevin dynamics simulations of the 2D Yukawa system to mimic 2D solid dusty plasmas under the shear deformation. In Sec. III, we determine the orientation-dependent shear modulus and yield stress from the stress-strain curves and the defect dynamics. We also provide our interpretation of the observed orientation-dependent yield using the calculated atomic elastic constants. Furthermore, we also present our found regular or reverse Bauschinger effects in 2D Yukawa solids. Finally, a brief summary is given in Sec. IV.

II. METHODS

We perform Langevin dynamics simulations of 2D Yukawa solids to mimic 2D solid dusty plasmas under the external shear deformation. The equation of motion for each particle i is [59]

$$m\ddot{\mathbf{r}}_i = -\nabla \Sigma \phi_{ij} - \nu m\dot{\mathbf{r}}_i + \zeta_i(t) + \mathbf{F}_{\rm ex}. \quad (1)$$

Here, the first term on the right-hand side is the interparticle Yukawa repulsion $\phi(r) = Q^2\exp(-r/\lambda_D)/4\pi\epsilon_0 r$, where r is the distance between two particles, Q is the charge on each particle, and λ_D is the screening length. The remaining three terms are the frictional gas drag [67], the Langevin random kicks [68], and the force from the externally applied shear, respectively. Our simulations are performed using Large-scale Atomic/Molecular Massively Parallel Simulator (LAMMPS) [69]. Note that, in addition to the Yukawa repulsion studied here, the bi-Yukawa [70] and even more complicated interactions [71] are also considered to mimic complex plasmas in other studies.

Traditionally [53,55], we use the coupling parameter Γ and the screening parameter κ to characterize the simulated 2D Yukawa systems. The coupling parameter Γ is defined as $\Gamma = Q^2/(4\pi\epsilon_0 a k_B T)$ [55], where T is the kinetic temperature of dust particles, k_B is the Boltzmann constant, and $a = (\pi n)^{-1/2}$ is the Wigner-Seitz radius for the 2D areal number density of n [23]. The screening parameter κ is defined as $\kappa = a/\lambda_D$. To normalize the time and length scales, we use the nominal 2D dusty plasma frequency $\omega_{\rm pd} = \sqrt{Q^2/2\pi\epsilon_0 m a^3}$ [65], and the Wigner-Seitz radius a, respectively.

As shown in Fig. 1, the external shear is applied within two shaded rectangular regions with the width of $10\,a$ in the $\pm x$ directions. In these two regions, the forces from the applied shear are expressed as $F_{\rm ex} = \pm F_0 m a\omega_{\rm pd}^2$, where F_0 is the magnitude of the force, while $ma\omega_{\rm pd}^2$ are the units of the force. Following the previous experimental studies with the shear modulation in 2D dusty plasmas [53,65], we choose the similar region between two laser modulation areas for the data analysis. To generate a larger uniform shear region, we specify the width between two laser manipulation areas to be $8a$, as shown in Fig. 1, larger than previous shear simulation studies in 2D dusty plasmas [55,59]. To study the anisotropic property of 2D Yukawa solids, the angle θ between the lattice orientation of the initial configuration and the shear direction, as marked in Fig. 1, is specified from $\theta = 0$ to $\theta = \pi/3$ with a step $\pi/36$ in our simulations. For each θ value, we keep the initial configuration of the 2D Yukawa solid unchanged, while varying the amplitude of $F_{\rm ex}$ slightly to obtain different shear deformation processes for the variation of various physical quantities in the latter data analysis. For example, the value of F_0 varies from 0.0028–0.0036 for $\theta = 0$, while it varies from 0.0048–0.0056 for $\theta = \pi/6$.

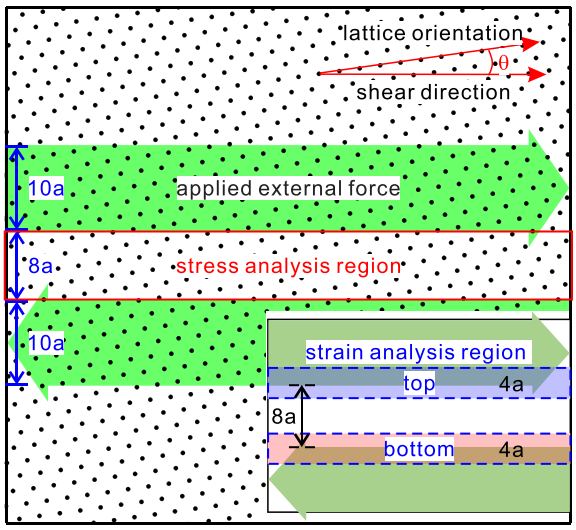

FIG. 1. Sketch of shear deformation of a 2D Yukawa solid under external modulations in our simulation. The constant shear force F_{ex} is applied within the two shaded regions in the opposite directions. We specify different lattice orientations in our simulations, where the angle between the shear direction and the principal axis of the lattice is labeled as θ. In the latter data analysis, the shear stress is calculated from the central region between two shaded regions, while the shear strain is determined from the displacement gradient calculated from the contribution of all particles inside the two strain analysis regions indicated by the dashed rectangle regions. Each simulation run always starts from the perfect crystal without defects in the central region of the simulation box. Note, only 6.25% of the total simulation box in the central portion is plotted here.

Here are some details of our simulations. The simulation box size is set as $243.792a \times 211.130a$, containing 16384 particles, and the periodic boundary conditions are used in the both x and y directions. Each simulation run always starts from a typical solid state [72] of $\Gamma = 2000$ and $\kappa = 0.5$, with a perfect crystal without defect in the central region of the simulation box, as shown in Fig. 1. Thus, we are able to exclude the effect of defects on the mechanical response of 2D Yukawa solids before the plastic deformation occurs. The gas damping rate ν is specified as $\nu = 0.036\omega_{\rm pd}$, a typical value in 2D dusty plasma experiments [53,65]. The integration time step is chosen as $1.41 \times 10^{-3}\omega_{\rm pd}^{-1}$, small enough to respond to the maximum shear deformation studied here. When the external shear forces are applied, the positions and velocities of all particles are recorded from the initial elastic regime to the latter plastic flow process.

To investigate the elastic and plastic mechanical behaviors of 2D Yukawa solids, we mainly focus on the relationship between the shear stress and shear strain, similar to Ref. [59]. The shear stress τ_{xy} is calculated as [55]

$$\tau_{xy} = \frac{1}{S}\sum_{i=1}^{M}\left[mv_{ix}v_{iy} - \frac{1}{2}\sum_{j\neq i}\frac{x_{ij}y_{ij}}{r_{ij}}\frac{\partial\phi(r_{ij})}{\partial r_{ij}}\right], \quad (2)$$

where S and M are the area and the number of particles in the analysis region, similar to Ref. [59]. The particle velocities v_{ix} and v_{iy} here are just the fluctuating portions, where the local drift velocity is removed, as in Ref. [59]. The stress is normalized by $\tau_0 = Q^2/4\pi\epsilon_0 a^3$. Note that, for various θ values, the number of particles in this analysis region is always larger than 600, so that the mechanical response of these particles under shear deformations is sufficient to reflect the collective properties of our simulated system.

The shear strain is defined as the displacement gradient along the shear direction [59], which is calculated as $\gamma = (u_{\text{top}} - u_{\text{bottom}})/\Delta d$. Here, u_{top} and u_{bottom} are the averaged displacements over all particle within the top and bottom regions with a width of $4a$, respectively, as indicated by two dashed rectangle regions in the inset of Fig. 1. The separation between the centers of the top and bottom regions is specified as $\Delta d = 8a$, which is just the same as the analysis region of the shear stress. For these two strain analysis regions, we use the cloud-in-cell algorithm [44] to average the displacement along the shear direction for all particles inside, as compared with their initial positions. Thus, the shear strain is calculated as the displacement gradient of the central portion between two applied external force regions. Note that we test that a slight change in the width of the strain analysis region does not have a significant effect on the obtained results of shear modulus.

III. RESULTS

A. Determination of yield point

Two typical stress-strain curves from the elastic to plastic deformations of the 2D Yukawa solid under the conditions of $\theta = \pi/12$ and $\theta = \pi/4$ are presented in Fig. 2(a). In the elastic deformation, for either $\theta = \pi/12$ or $\theta = \pi/4$, the stress-strain relationship is just a straight line with a constant slope until the shear stress reaches the proportional limit, as labeled by the circle in Fig. 2(a). The slope of the straight line of the stress-strain relationship represents the corresponding shear modulus. However, when the shear stress exceeds the proportional limit of the circle in Fig. 2(a), the curve of the stress-strain relationship starts to change to a different direction with either a steeper or a slower increasing rate, corresponding to the shear hardening and softening features, respectively. Note that these shear hardening and softening features still exist within the elastic limit before the maximum shear stress, at which our studied 2D Yukawa solids are able to recover their original states after unloading.

As shown in Fig. 2(a), for our studied 2D Yukawa solids, the difference between the proportional limit and the elastic limit is significant, so that it is easy to distinguish them. In fact, for most materials, such as most metals [73] and some soft matters [74], the proportional limit, the elastic limit, and the yield stress are very close, as a result it is quite difficult to distinguish their exact values from the stress-strain diagram [73]. In Fig. 2(a), the yield stress and the elastic limit are very close around the maximum of the shear stress, so that we cannot distinguish them directly from the stress-strain curve. To accurately determine the yield stress of 2D Yukawa solids, we need to use other sensitive diagnostics obtained from individual particles.

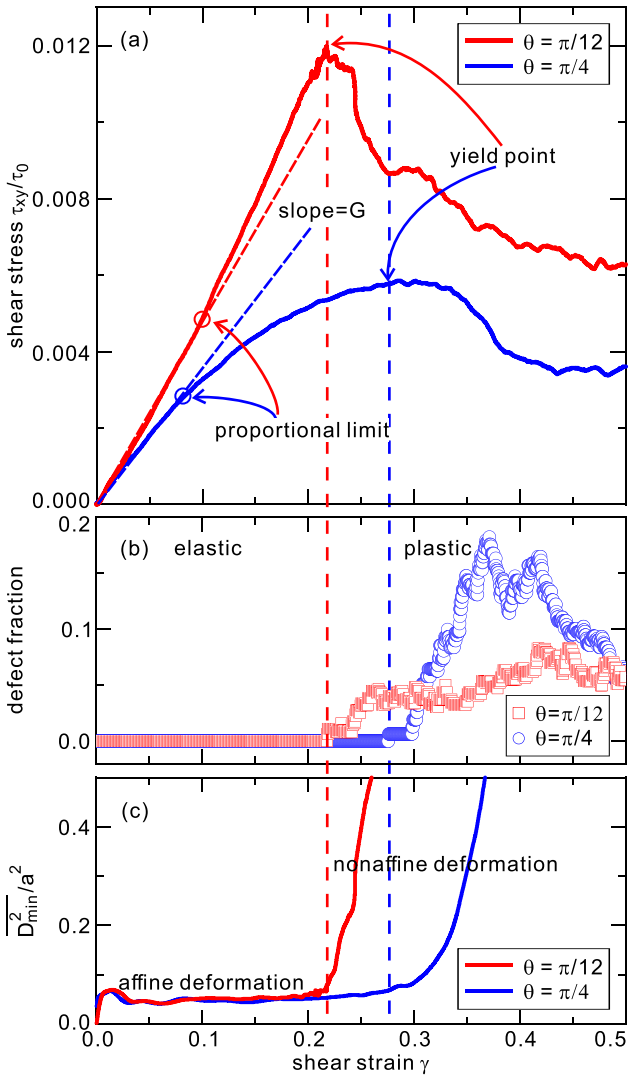

FIG. 2. (a) Calculated shear stress τ_{xy}, (b) defect fraction, and (c) the average deviation from the affine displacement $\overline{D^2_{\text{min}}}$ as the functions of the shear strain γ of the 2D Yukawa solid, for two typical lattice orientation angles of $\theta = \pi/12$ and $\theta = \pi/4$. In our data analysis, the shear modulus G is determined from the slope of the stress-strain response curve within the proportional limit, as labeled in (a). The yield stress is obtained from the location where the plastic deformation just occurs, corresponding to the generation of defects. Thus, at the yield point, dislocations appear inside the analysis region, so that the defect fraction is not zero anymore as in (b), corresponding to the approximate maximum of τ_{xy} in (a), as well as the transition point of D^2_{min} in (c), as the two vertical dashed lines shown in (a)–(c).

To determine the yield point of the 2D Yukawa solid more precisely, here we use two microscopic diagnostics of the defect fraction and the deviation from the affine displacement [75], respectively, as shown in Figs. 2(b) and 2(c). Since the plastic deformation is directly related to the dislocation motion for crystals [4], the yield point should be able to be accurately determined from the dislocation dynamics. Here, we calculate the time series of the defect fraction of the total stress analysis region during the whole deformation process, as shown in Fig. 2(b) for the conditions of $\theta = \pi/12$ and $\theta = \pi/4$, respectively. Clearly, for either $\theta = \pi/12$ or $\theta = \pi/4$, the defect fraction is always zero during the initial elastic deformation, since the initial configuration is defect free. With the further increase of γ, the defect fraction is not zero anymore, and the defect fraction starts to increase rapidly, indicating that the system reaches a steady plastic deformation. Since the initial configuration of the analysis region is defect free, it is reasonable to choose the condition where defects just appear as the yield point, as indicated by two vertical dashed lines in Fig. 2. From the stress-strain curves in Fig. 2(a), for each yield point determined by the transition point from zero to nonzero of the defect fraction in Fig. 2(b), the corresponding shear yield stress τ_{yield} is always nearly the maximum of shear stress. Note that to determine the defect fraction, we calculate Voronoi diagrams at all moments using all particle positions in the analysis region, where the defect fraction is defined as the number ratio of non-six-sided polygons to all polygons.

Another diagnostic is the deviation from the affine displacement D^2_{min} [75], which is commonly used in amorphous solids to quantify the nonaffine deformation. For each particle i, D^2_{min} is defined as the minimum over all possible linear deformation tensors $\boldsymbol{\varepsilon}$ of [75]

$$D^2(i,\gamma,0) = \sum_j [\mathbf{r}_{ij}(\gamma) - (\mathbf{I}+\boldsymbol{\varepsilon})\cdot\mathbf{r}_{ij}(0)]^2. \tag{3}$$

Here, the index j denotes nearest neighbors of the reference particle i, $\mathbf{I}$ is the identity matrix, $\mathbf{r}_{ij}(\gamma)$ is the distance vector between the particles i and j in a snapshot of the specified γ value. Here, we choose the initial configuration of $\gamma = 0$ as the reference configuration without any deformations. The value of D^2_{min} is very sensitive to the local irreversible shear deformation [75,76], which is able to identify the yield point. Instead of observing the distribution of $D^2_{\text{min}}(i)$ for one snapshot like in Refs. [75,76], we take the average of $D^2_{\text{min}}(i)$ for all particles in the analysis region to quantify the nonaffine deformation of the whole system, calculated as $\overline{D^2_{\text{min}}} = \frac{1}{M}\sum_{i=1}^{M} D^2_{\text{min}}(i)$.

To investigate the relationship between the plastic deformation and the nonaffine displacement, we calculate the time series of the averaged deviation from the affine displacement $\overline{D^2_{\text{min}}}$, as presented in Fig. 2(c). For either $\theta = \pi/12$ or $\theta = \pi/4$, the value of $\overline{D^2_{\text{min}}}$ nearly keeps $\approx$0.05 during the elastic deformation. This low value of $\overline{D^2_{\text{min}}}$ indicates that the displacements of most particles are almost reversible, i.e., the deformation is recoverable for the elastic deformation. When the shear strain γ further increases, the calculated $\overline{D^2_{\text{min}}}$ increases suddenly and sharply, suggesting the significant irreversible deformation occurs. The point where the value of $\overline{D^2_{\text{min}}}$ begins to increase dramatically just corresponds to the yield point determined from the defect fraction, i.e., the vertical dashed lines in Fig. 2. Our observed results above indicate that, in addition to the defect fraction in Fig. 2(b), the average deviation from the affine displacement $\overline{D^2_{\text{min}}}$ in Fig. 2(c) is also sensitive enough to determine the yield point of 2D Yukawa solids.

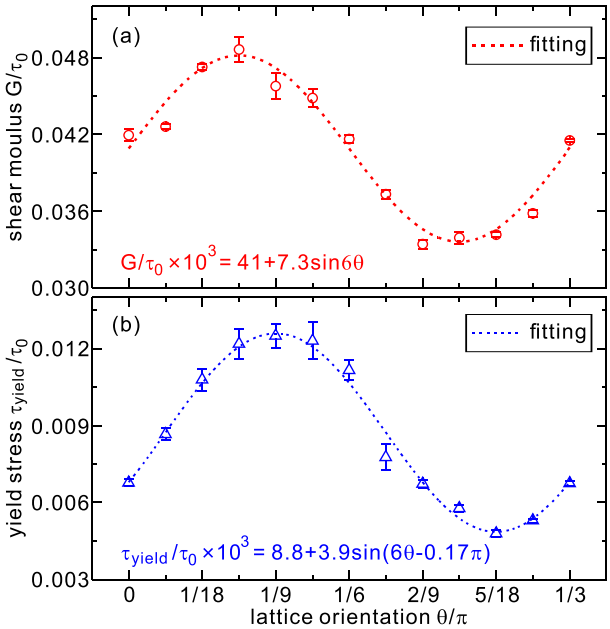

FIG. 3. (a) Obtained orientation-dependent shear modulus $G(\theta)$ and (b) yield stress $\tau_{\text{yield}}(\theta)$. In (a), the shear modulus varies approximately sinusoidally with the angle θ, as the fitting curve shown. While choosing $G(\theta = 0)$ as the reference, then the $G(\theta)$ results exhibit the significant hardening and softening features in the ranges of $0 < \theta < \pi/6$ and $\pi/6 < \theta < \pi/3$, respectively. In (b), the variation trend of the yield stress with θ is also approximately sinusoidal, while there is a phase difference 0.17π between the variations of $\tau_{\text{yield}}(\theta)$ and $G(\theta)$, as the fitting curve shown there.

B. Orientation-dependent shear modulus and yield stress

As the major result, we discover anisotropic behaviors of the shear modulus G and yield stress τ_{yield} of a 2D Yukawa hexagonal crystal, as well as our obtained dependence of G and τ_{yield} on the lattice orientation θ presented in Fig. 3. In Fig. 3(a), when θ increases from 0 to $\pi/3$, the obtained orientation-dependent shear modulus $G(\theta)$ varies approximately sinusoidally with the angle θ. We find that the obtained $G(\theta)$ is able to be fitted as $G/\tau_0 \times 10^3 = 41 + 7.3\sin 6\theta$. Here, due to the hexagonal symmetry of the 2D Yukawa lattice, the period of the orientation angle θ in the fitting expression is specified to be $\pi/3$. For our specified $\kappa = 0.5$, from the expression of the sound speed of a perfect 2D Yukawa crystal [77], the theoretical transverse sound speed C_T is about $0.25a\omega_{pd}$. As a result, the corresponding theoretical shear modulus of the 2D Yukawa crystal is $G_0 = \rho C_T^2 = 0.040\tau_0$ [58], where ρ is the mass density. This theoretical value of the shear modulus well agrees with the value of $G \approx 0.042\tau_0$ when $\theta = 0$, $\theta = \pi/6$, and $\theta = \pi/3$ in Fig. 3.

The maximum of the shear modulus in Fig. 3 occurs when $\theta = \pi/12$, i.e.,$G(\theta = \pi/12) = 0.049\tau_0$ is substantially larger than $G_0 = 0.040\tau_0$, while its minimum occurs when $\theta = 2\pi/9$ with the corresponding value of only $0.033\tau_0$. While choosing $G(\theta = 0)$ as the reference, the orientation-dependent $G(\theta)$ exhibits the significant shear hardening and softening properties in the ranges of $0 < \theta < \pi/6$ and $\pi/6 < \theta < \pi/3$, respectively.

The orientation-dependent yield stress $\tau_{\text{yield}}(\theta)$ of the 2D Yukawa solid also varies approximately sinusoidally with the orientation angle θ, as shown in Fig. 3(b). Similar to Fig. 3(a), since the period of the orientation angle θ is $\pi/3$, we find that the orientation-dependent yield stress $\tau_{\text{yield}}(\theta)$ can be fitted as $\tau_{\text{yield}}/\tau_0 \times 10^3 = 8.8 + 3.9\sin(6\theta - 0.17\pi)$, with a phase difference 0.17π behind the shear modulus $G(\theta)$. In Fig. 3(b), as θ increases from 0 to $\pi/9$, the yield stress τ_{yield} increases from $0.00677\tau_0$ to $0.0125\tau_0$. When θ increases from $\pi/9$ to $5\pi/18$, the value of τ_{yield} decreases from $0.0125\tau_0$ to $0.00479\tau_0$. The maximum of $\tau_{\text{yield}}(\theta)$ is about 2.6 times larger than its minimum, indicating that the effect of the lattice orientation on the yield stress in Fig. 3(b) is much more significant than that on the shear modulus in Fig. 3(a). The error bars in Fig. 3 are obtained from five different runs for each θ. Note that this anisotropic yield behavior of 2D Yukawa solids is further confirmed under various conditions, as presented in Ref. [78].

To quantitatively interpret the observed anisotropic behaviors of the shear modulus and the yield stress above, we calculate the time series of the atomic elastic constant C_{xyxy} for various lattice orientations, as presented in Fig. 4(a). As in Eq. (3) of Ref. [59], we calculate the atomic elastic constant $C_{xyxy}(i)$ from individual particle positions, and then average $C_{xyxy}(i)$ over all particles in the stress analysis region. In Fig. 4(a), the obtained time series of C_{xyxy} exhibit two completely different variation trends for various θ values, corresponding to either the shear hardening or softening features. Especially for the conditions of the maximum and minimum of $\tau_{\text{yield}}(\theta)$, i.e., $\theta = \pi/9$ and $5\pi/18$, the C_{xyxy} results change with γ the most significantly. The results in Fig. 4(a) indicate that the anisotropic yield may be caused by the anisotropic elasticity of our studied 2D Yukawa solids.

To further investigate the results of the yield stress in Fig. 3(b), we extract the value of C_{xyxy} corresponding to the yield point for different θ values, as the star symbols presented in Fig. 4. We find that the variation trend of C_{xyxy} with θ under $\gamma = \gamma_{\text{yield}}$ is also able to be fitted as a sinusoidal form of $C_{xyxy}/\tau_0 \times 10^3 = 38 + 42\sin(6\theta - 0.23\pi)$, with the phase angle slightly behind that of the orientation-dependent yield stress $\tau_{\text{yield}}(\theta)$ in Fig. 3(b). To compare with the orientation-dependent shear modulus in Fig. 3(a), we also extract the value of C_{xyxy} when γ is specified as 0.1, always within the proportional limit for different θ values. As shown in Fig. 4(b), the value of C_{xyxy} for $\gamma = 0.1$ also varies sinusoidally with the fitting expression of $C_{xyxy}/\tau_0 \times 10^3 = 42 + 18\sin(6\theta - 0.09\pi)$. The phase difference between the variation of C_{xyxy} with θ under the conditions of $\gamma = 0.1$ and $\gamma = \gamma_{\text{yield}}$ is 0.14π, well consistent with the phase difference of 0.17π between the orientation-dependent shear modulus $G(\theta)$ and yield stress $\tau_{\text{yield}}(\theta)$ in Fig. 3. The results in Figs. 3 and 4 further suggest that the orientation-dependent yield in 2D Yukawa solids is caused by their elastic anisotropy.

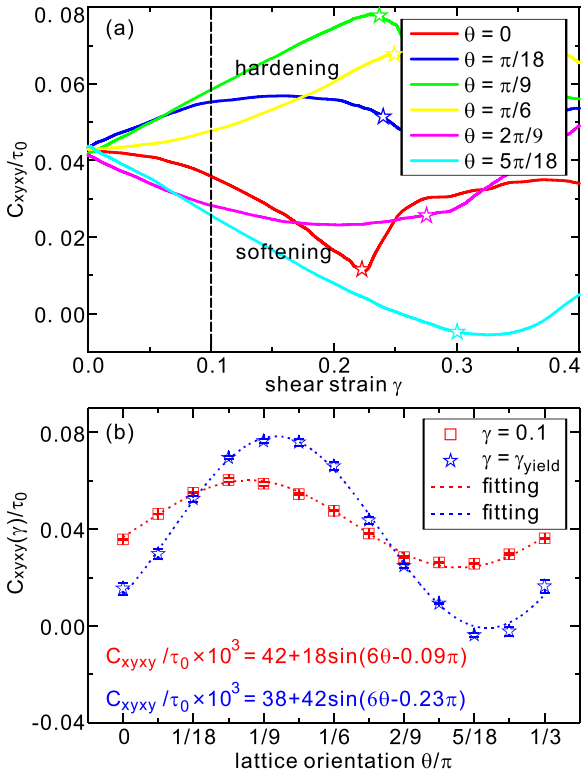

FIG. 4. (a) Calculated results of the elastic constant C_{xyxy} of one particle in 2D Yukawa solids as functions of γ for various θ values, and (b) the results of C_{xyxy} under specified γ values for different θ values. In (a), with the increase of the shear strain γ, the elastic constant C_{xyxy} exhibits either the shear hardening or the shear softening, for different orientation angles. In (a), the star symbol in each C_{xyxy} curve indicates the yield point determined by the increase of the defect fraction, and the corresponding strain value is labeled as γ_{yield}. We also draw a dashed line of $\gamma = 0.1$ within the typical proportional limit. In (b), for $\gamma = 0.1$ and $\gamma = \gamma_{\text{yield}}$, the variations of C_{xyxy} both vary approximately sinusoidally with θ, in good agreement with the shear modulus and yield stress in Fig. 3, respectively.

From our understanding, for our studied 2D defect-free Yukawa crystal here, the yield stress is equivalent to the critical shear stress, under which the first dislocation is generated. In this case, the yield behavior corresponds a rigid slip between any two adjacent atomic layers, so that the theoretical yield strength can be estimated as $\tau_t = \frac{G}{2\pi}\frac{b}{d}$ [2], where b is the lattice constant, and d is the spacing between two adjacent atomic layers. For a 2D triangular lattice of our studied 2D Yukawa solids, the ratio between b and d is just $2/\sqrt{3}$. Substituting this ratio and the theoretical shear modulus G_0 of the 2D Yukawa crystal into the above equation, we obtain the corresponding theoretical yield strength of $\tau_t/\tau_0 = 7.35 \times 10^{-3}$. For our current theoretical derivation, the lattice orientation is the same as the shear direction, i.e., $\theta = 0$, so that we are able to compare the obtained yield stress $\tau_{\text{yield}}(\theta = 0)$ with this theoretically derived yield strength τ_t. We find that the theoretically derived value $\tau_t/\tau_0 = 7.35 \times 10^{-3}$ agrees with the yield stress of $\tau_{\text{yield}}(\theta = 0)/\tau_0 = 6.77 \times 10^{-3}$ obtained from Fig. 3(b). This agreement further suggests that our ob-

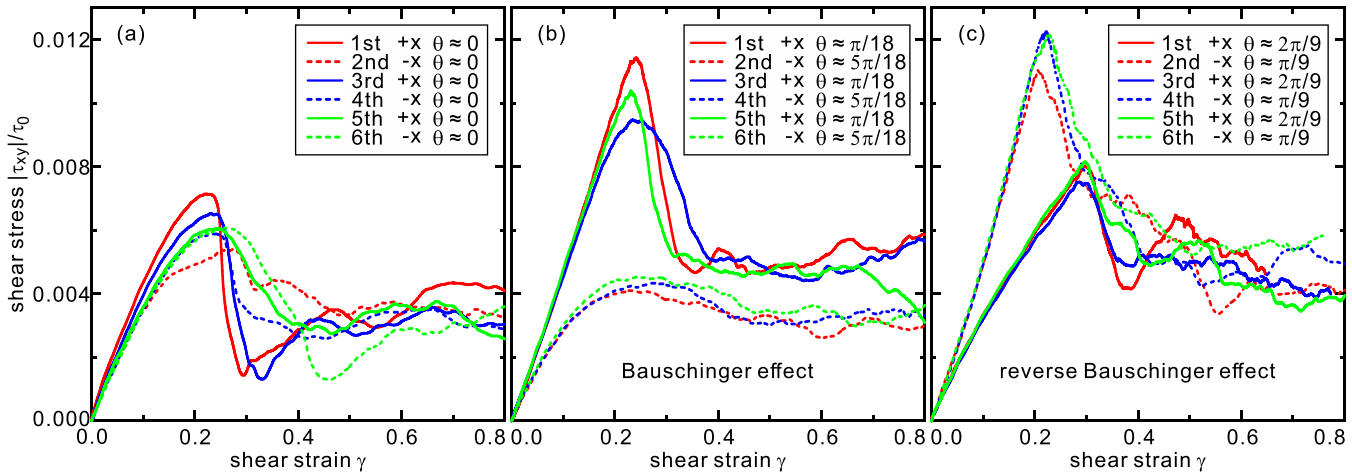

FIG. 5. Stress-strain response during three forward (solid lines) and three backward (dashed lines) shear modulations for the initial orientation angle of (a) $\theta \approx 0$, (b) $\theta \approx \pi/18$, and (c) $\theta \approx 2\pi/9$, respectively. In the first forward shear deformation cycle, the shear deformation is applied in the $+x$ direction until the plastic deformation is achieved, then the applied deformation is completely released, so that the shear stress is fully relaxed to nearly zero. Next, the reverse shear deformation is applied and released similarly. This back and forth deformation is performed continuously several times. For the initial configuration of $\theta \approx 0$ in (a), the stress-strain curves obtained by multiple repeating shears are nearly the same, i.e., almost no significant Bauschinger effect is observed. For the initial configuration of $\theta \approx \pi/18$ in (b), the yield stresses of forward shears are much larger than those of reverse shears, i.e., the significant Bauschinger effect is observed. For the initial configuration of $\theta \approx 2\pi/9$ in (c), the yield stresses under forward shears are always lower than those under reverse shears, i.e., a reverse Bauschinger effect is clearly observed.

tained yield stress is just the critical shear stress to generate dislocations in 2D Yukawa solids.

C. Regular and reverse Bauschinger effects

The Bauschinger effect is a plastic behavior directly related to the yield stress, which is generally considered to be strongly dependent on the loading history. Especially during cyclic loading, the Bauschinger effect may have a significant influence on some mechanical properties of systems, such as the yield strength. Thus, we would like to report our obtained relationship between the anisotropic yield and Bauschinger effect next.

To examine the existence of the possible Bauschinger effect in 2D Yukawa solids, we also apply the repeating shear deformations in the forward and reverse cycles. The shear deformation cycles are performed as follows. The first forward shear with a uniform amplitude is applied in the $+x$ direction until the system reaches the plastic deformation, then the applied shear is removed completely, so that the shear stress is relaxed to nearly zero. Next, the reverse shear with the same uniform amplitude is applied in the $-x$ direction to generate the plastic deformation in the opposite direction, and then the shear deformation is completely removed similarly, so that the shear stress is relaxed to zero again. In our simulations, these forward and reverse shear deformations are continuously performed several times on the 2D Yukawa solid as described above.

The stress-strain response curves during three forward and backward shear modulations for the three typical initial θ values are presented in Fig. 5. For the initial configuration of $\theta \approx 0$ in Fig. 5(a), during the three forward and reverse shear deformations, the orientation angle θ between the shear direction and the lattice orientation in the initial configuration does not change at all. As a result, the obtained stress-strain curves are nearly unchanged, suggesting that there is almost no significant Bauschinger effect at all. Although the initial configuration is defect free before the shear deformation is applied, during subsequent shear modulations, a few generated dislocations always exist, no matter how the shear stress is relaxed. The results in Fig. 5(a) also indicate that the presence of defects in the second and third cycles does not have a significant effect on the yield stress. Note that we also perform test runs with more shear cycles, as reported in Ref. [78], and the resulting stress-strain curves are almost the same as those in Fig. 5, no matter how the number of shear cycles increases.

In Fig. 5(b), we observe a significant Bauschinger effect for initial configuration of $\theta \approx \pi/18$. In this case, the angle θ in the initial configuration is about $\pi/18$ for the forward shear deformation, while for the latter reverse shear deformation, the angle θ changes to $5\pi/18$ immediately. In Fig. 5(b), for either the forward or reverse shear deformation, we find that three obtained stress-strain curves almost overlap together. Furthermore, the yield stress of the forward shear is much larger than that of the reverse shear, just corresponding to the significant Bauschinger effect. In fact, during several shear deformation cycles, the lattice orientation does not change, the sudden change of θ is just due to the reversal of the shear direction. Thus, our observed Bauschinger effect is mainly induced by the orientation-dependent yield of the 2D Yukawa solid.

In addition, we also observe that there is a reverse Bauschinger effect for 2D Yukawa solids, as shown in Fig. 5(c). Here, the initial value of θ is about $2\pi/9$ for the forward shear deformation, while this value changes to $\pi/9$ immediately for the latter reverse shear deformation. From the obtained stress-strain curves in Fig. 5(c), the yield stress of the forward shear deformation is obviously smaller than

that of the reverse shear, exhibiting the completely opposite property as compared with Fig. 5(b), i.e., a significant reverse Bauschinger effect. Similarly, the observed reverse Bauschinger effect is also caused by the orientation-dependent yield of the 2D Yukawa solid. Our findings in Fig. 5 provide a reasonable interpretation of the Bauschinger effect in single crystals. In 2D dusty plasma experiments, it is feasible to apply the forward and reverse shear deformations using laser manipulations, so that our observed regular and reverse Bauschinger effects may be experimentally verified in future.

IV. SUMMARY

We perform Langevin dynamics simulations of 2D Yukawa solids to investigate the orientation-dependent yield and the corresponding Bauschinger effects in solid 2D dusty plasmas under shear deformations. From the obtained stress-strain curves and the resulting defect fractions, we determine the yield stress of 2D Yukawa solids under different conditions. We discover that the observed yield behavior in 2D Yukawa solids is accompanied by the formation of new dislocations, resulting in the rapid increase of the nonaffine displacement. We find that both the shear modulus and yield stress are strongly dependent on the lattice orientation, exhibiting the significant anisotropic behaviors. To interpret the underlying mechanism, we calculate the atomic elastic constant, whose orientation dependence almost completely agrees with those of the shear modulus and yield stress. We also find that, for different initial lattice orientations, the 2D Yukawa solid exhibits the significant regular or reverse Bauschinger effects, or even non-Bauschinger effect. The regular and reverse Bauschinger effects observed in our simulations may be verified in future 2D dusty plasma experiments, since the shear deformation cycle is able to be achieved using the laser manipulation method.

ACKNOWLEDGMENTS

Work was supported by the National Natural Science Foundation of China under Grants No. 12175159, No. 12347110, and No. 12305220, the 1000 Youth Talents Plan, startup funds from Soochow University, the Postdoctoral Fellowship Program of CPSF under Grant No. GZC20231901, and the Priority Academic Program Development (PAPD) of Jiangsu Higher Education Institutions.

[1] E. J. Hearn, *Mechanics of Materials: The Mechanics of Elastic and Plastic Deformation of Solids and Structural Materials* (Elsevier, Amsterdam, 1997).

[2] I. Kovács and L. Zsoldos, *Dislocations and Plastic Deformation: International Series of Monographs in Natural Philosophy* (Elsevier, Amsterdam, 2016).

[3] J. Lubliner, *Plasticity Theory* (Dover Books on Engineering, Berkeley, 2006).

[4] T. Suzuki, S. Takeuchi, and H. Yoshinaga, *Dislocation Dynamics and Plasticity* (Springer, Heidelberg, 1991).

[5] P. D. Ispánovity, I. Groma, G. Györgyi, F. F. Csikor, and D. Weygand, Submicron plasticity: Yield stress, dislocation avalanches, and velocity distribution, Phys. Rev. Lett. **105**, 085503 (2010).

[6] R. A. Hill, A theory of the yielding and plastic flow of anisotropic metals, Proc. R. Soc. Lond. A **193**, 281 (1948).

[7] J. Bauschinger, On the change of the position of elastic limit of iron and steel under cyclic variation of stress, Mit. mech.-tech. Lab. kgl. TH Muenchen **13**, 1 (1886).

[8] D. Zhu, H. Zhang, and D. Y. Li, Molecular dynamics simulation of Bauschinger's effect in deformed copper single crystal in different strain ranges, J. Appl. Phys. **110**, 124911 (2011).

[9] A. A. Mamun, R. J. Moat, J. Kelleher, and P. J. Bouchard, Origin of the Bauschinger effect in a polycrystalline material, Mater. Sci. Eng. A **707**, 576 (2017).

[10] D. J. A. Senden, J. A. W. van Dommelen, and L. E. Govaert, Strain hardening and its relation to Bauschinger effects in oriented polymers, J. Polym. Sci. Polym. Phys. Ed. **48**, 1483 (2010).

[11] S. Patinet, A. Barbot, M. Lerbinger, D. Vandembroucq, and A. Lemaître, Origin of the Bauschinger effect in amorphous solids, Phys. Rev. Lett. **124**, 205503 (2020).

[12] F. Frahsa, A. K. Bhattacharjee, J. Horbach, M. Fuchs, and T. Voigtmann, On the Bauschinger effect in supercooled melts under shear: Results from mode coupling theory and molecular dynamics simulations, J. Chem. Phys. **138**, 12A513 (2013).

[13] D. Kushnir, C. Ruscher, E. Bartsch, F. Thalmann, and P. Hébraud, Stress overshoot, hysteresis, and the Bauschinger effect in sheared dense colloidal suspensions, Phys. Rev. E **106**, 034611 (2022).

[14] S. Deboeuf, L. Ducloué, N. Lenoir, and G. Ovarlez, A mechanism of strain hardening and Bauschinger effect: Shear-history-dependent microstructure of elasto-plastic suspensions, Soft Matter **18**, 8756 (2022).

[15] Z. Zheng, R. Li, M. Zhan, G. Yuan, H. Zhang, Y. Lei, and D. S. Balint, The effect of strain rate asymmetry on the Bauschinger effect: A discrete dislocation plasticity analysis, J. Mater. Res. Technol. **16**, 1904 (2022).

[16] A. Seeger, J. Diehl, S. Mader, and H. Rebstock, Work-hardening and work-softening of face-centred cubic metal crystals, Philos. Mag. **2**, 323 (1957).

[17] S. Karmakar, E. Lerner, and I. Procaccia, Plasticity-induced anisotropy in amorphous solids: The Bauschinger effect, Phys. Rev. E **82**, 026104 (2010).

[18] H. M. Thomas and G. E. Morfill, Melting dynamics of a plasma crystal, Nature (London) **379**, 806 (1996).

[19] L. I. W. Juan, C. Chiang, and J. Chu, Microscopic particle motions in strongly coupled dusty plasmas, Science **272**, 1626 (1996).

[20] A. Melzer, A. Homann, and A. Piel, Experimental investigation of the melting transition of the plasma crystal, Phys. Rev. E **53**, 2757 (1996).

[21] M. S. Murillo, Critical wave vectors for transverse modes in

strongly coupled dusty plasmas, Phys. Rev. Lett. **85**, 2514 (2000).
[22] R. L. Merlino and J. A. Goree, Dusty plasmas in the laboratory, industry, and space, Phys. Today **57**(7), 32 (2004).
[23] G. J. Kalman, P. Hartmann, Z. Donkó, and M. Rosenberg, Two-dimensional Yukawa liquids: Correlation and dynamics, Phys. Rev. Lett. **92**, 065001 (2004).
[24] V. E. Fortov, A. V. Ivlev, S. A. Khrapak, A. G. Khrapak, and G. E. Morfill, Complex (dusty) plasmas: Current status, open issues, perspectives, Phys. Rep. **421**, 1 (2005).
[25] G. E. Morfill and A. V. Ivlev, Complex plasmas: An interdisciplinary research field, Rev. Mod. Phys. **81**, 1353 (2009).
[26] A. Piel, *Plasma Physics* (Springer, Heidelberg, 2010).
[27] M. Bonitz, C. Henning, and D. Block, Complex plasmas: A laboratory for strong correlations, Rep. Prog. Phys. **73**, 066501 (2010).
[28] A. Melzer, A. Schella, J. Schablinski, D. Block, and A. Piel, Analyzing the liquid state of two-dimensional dust clusters, Phys. Rev. E **87**, 033107 (2013).
[29] E. Thomas Jr., U. Konopka, R. L. Merlino, and M. Rosenberg, Initial measurements of two-and three-dimensional ordering, waves, and plasma filamentation in the magnetized dusty plasma experiment, Phys. Plasmas **23**, 055701 (2016).
[30] S. Jaiswal, T. Hall, S. LeBlanc, R. Mukherjee, and E. Thomas, Effect of magnetic field on the phase transition in a dusty plasma, Phys. Plasmas **24**, 113703 (2017).
[31] C. R. Du, V. Nosenko, H. M. Thomas, Y. F. Lin, G. E. Morfill, and A. V. Ivlev, Slow dynamics in a quasi-two-dimensional binary complex plasma, Phys. Rev. Lett. **123**, 185002 (2019).
[32] F. Wieben and D. Block, Entropy measurement in strongly coupled complex plasmas, Phys. Rev. Lett. **123**, 225001 (2019).
[33] Y. He, B. Ai, C. Dai, C. Song, R. Wang, W. Sun, F. Liu, and Y. Feng, Experimental demonstration of a dusty plasma ratchet rectification and its reversal, Phys. Rev. Lett. **124**, 075001 (2020).
[34] W. Yu, J. Cho, and J. C. Burton, Extracting forces from noisy dynamics in dusty plasmas, Phys. Rev. E **106**, 035303 (2022).
[35] S. Singh, P. Bandyopadhyay, K. Kumar, and A. Sen, Square lattice formation in a monodisperse complex plasma, Phys. Rev. Lett. **129**, 115003 (2022).
[36] J. Beckers, J. Berndt, D. Block, M. Bonitz, P. J. Bruggeman, L. Couëdel, G. L. Delzanno, Y. Feng, R. Gopalakrishnan, F. Greiner, P. Hartmann, M. Horányi, H. Kersten, C. A. Knapek, U. Konopka, U. Kortshagen, E. G. Kostadinova, E. Kovačević, S. I. Krasheninnikov, I. Mann, D. Mariotti, L. S. Matthews, A. Melzer, M. van de Kerkhof *et al.*, Physics and applications of dusty plasmas: The Perspectives, Phys. Plasmas **30**, 120601 (2023).
[37] Y. Feng, J. Goree, and B. Liu, Solid superheating observed in two-dimensional strongly coupled dusty plasma, Phys. Rev. Lett. **100**, 205007 (2008).
[38] K. Qiao, J. Kong, J. Carmona-Reyes, L. S. Matthews, and T. W. Hyde, Mode coupling and resonance instabilities in quasi-two-dimensional dust clusters in complex plasmas, Phys. Rev. E **90**, 033109 (2014).
[39] L. Couëdel and V. Nosenko, Stability of two-dimensional complex plasma monolayers in asymmetric capacitively coupled radio-frequency discharges, Phys. Rev. E **105**, 015210 (2022).
[40] Z. Donkó, J. Goree, P. Hartmann, and K. Kutasi, Shear viscosity and shear thinning in two-dimensional Yukawa liquids, Phys. Rev. Lett. **96**, 145003 (2006).
[41] C. L. Chan and I. Lin, Viscoelastic response of mesoscopic dusty-plasma liquids, Phys. Rev. Lett. **98**, 105002 (2007).
[42] B. Liu and J. Goree, Superdiffusion and non-Gaussian statistics in a driven-dissipative 2D dusty plasma, Phys. Rev. Lett. **100**, 055003 (2008).
[43] T. Ott and M. Bonitz, Is diffusion anomalous in two-dimensional Yukawa liquids, Phys. Rev. Lett. **103**, 195001 (2009).
[44] Y. Feng, J. Goree, and B. Liu, Viscoelasticity of 2D liquids quantified in a dusty plasma experiment, Phys. Rev. Lett. **105**, 025002 (2010).
[45] F. Lucco Castello and P. Tolias, Structure and thermodynamics of two-dimensional Yukawa liquids, Phys. Rev. E **103**, 063205 (2021).
[46] M. S. Murillo, Strongly coupled plasma physics and high energy-density matter, Phys. Plasmas **11**, 2964 (2004).
[47] A. Melzer, A. Schella, J. Schablinski, D. Block, and A. Piel, Instantaneous normal mode analysis of melting of finite dust clusters, Phys. Rev. Lett. **108**, 225001 (2012).
[48] P. Hartmann, A. Douglass, J. C. Reyes, L. S. Matthews, T. W. Hyde, A. Kovács, and Z. Donkó, Crystallization dynamics of a single layer complex plasma, Phys. Rev. Lett. **105**, 115004 (2010).
[49] E. Thomas Jr., B. Lynch, U. Konopka, R. L. Merlino, and M. Rosenberg, Observations of imposed ordered structures in a dusty plasma at high magnetic field, Phys. Plasmas **22**, 030701 (2015).
[50] J. D. Williams, E. Thomas, L. Couëdel, A. V. Ivlev, S. K. Zhdanov, V. Nosenko, H. M. Thomas, and G. E. Morfill, Kinetics of the melting front in two-dimensional plasma crystals: complementary analysis with the particle image and particle tracking velocimetries, Phys. Rev. E **86**, 046401 (2012).
[51] C. Durniak and D. Samsonov, Plastic deformations in complex plasmas, Phys. Rev. Lett. **106**, 175001 (2011).
[52] P. Hartmann, A. Z. Kovács, A. M. Douglass, J. C. Reyes, L. S. Matthews, and T. W. Hyde, Slow plastic creep of 2D dusty plasma solids, Phys. Rev. Lett. **113**, 025002 (2014).
[53] S. Lu, D. Huang, and Y. Feng, Plastic strain rate quantified from dislocation dynamics in dusty plasma shear flows, Phys. Rev. E **103**, 063214 (2021).
[54] A. Piel, V. Nosenko, and J. Goree, Experiments and molecular-dynamics simulation of elastic waves in a plasma crystal radiated from a small dipole source, Phys. Rev. Lett. **89**, 085004 (2002).
[55] B. Liu and J. Goree, Determination of yield stress of 2D (Yukawa) dusty plasma, Phys. Plasmas **24**, 103702 (2017).
[56] W. Li, W. Lin, and Y. Feng, Bulk modulus of two-dimensional liquid dusty plasmas and its application, Phys. Plasmas **24**, 043702 (2017).
[57] S. Khrapak and B. Klumov, High-frequency elastic moduli of two-dimensional Yukawa fluids and solids, Phys. Plasmas **25**, 033706 (2018).
[58] K. Wang, D. Huang, and Y. Feng, Shear modulus of two-dimensional Yukawa or dusty-plasma solids obtained from the viscoelasticity in the liquid state, Phys. Rev. E **99**, 063206 (2019).
[59] S. Lu, D. Huang, and Y. Feng, Shear softening and hardening

of a two-dimensional Yukawa solid, Phys. Rev. E **105**, 035203 (2022).

[60] V. Nosenko, A. V. Ivlev, and G. E. Morfill, Anisotropic shear melting and recrystallization of a two-dimensional complex plasma, Phys. Rev. E **87**, 043115 (2013).

[61] V. Nosenko, S. Zhdanov, and G. E. Morfill, Supersonic dislocations observed in a plasma crystal, Phys. Rev. Lett. **99**, 025002 (2007).

[62] V. Nosenko, G. E. Morfill, and P. Rosakis, The speed-stress relation for dislocations in a plasma crystal, Phys. Rev. Lett. **106**, 155002 (2011).

[63] C. L. Chan, W. Y. Woon, and I. Lin, Shear banding in mesoscopic dusty plasma liquids, Phys. Rev. Lett. **93**, 220602 (2004).

[64] V. Nosenko and J. Goree, Shear flows and shear viscosity in a two-dimensional Yukawa system (dusty plasma), Phys. Rev. Lett. **93**, 155004 (2004).

[65] Y. Feng, J. Goree, and B. Liu, Viscous heating in a dusty plasma flow, Phys. Rev. Lett. **109**, 185002 (2012).

[66] Y. Feng, J. Goree, and B. Liu, Evolution of shear-induced melting in a dusty plasma, Phys. Rev. Lett. **104**, 165003 (2010).

[67] B. A. Klumov and G. E. Morfill, Structural properties of complex (dusty) plasma upon crystallization and melting, JETP Lett. **90**, 444 (2009).

[68] Y. Feng, B. Liu, and J. Goree, Rapid heating and cooling in two-dimensional Yukawa systems, Phys. Rev. E **78**, 026415 (2008).

[69] S. Plimpton, Fast parallel algorithms for short-range molecular-dynamics, J. Comput. Phys. **117**, 1 (1995); http://lammps.sandia.gov.

[70] F. Lucco Castello, P. Tolias, J. S. Hansen, and J. C. Dyre, Isomorph invariance and thermodynamics of repulsive dense bi-Yukawa one-component plasmas, Phys. Plasmas **26**, 053705 (2019).

[71] A. V. Zampetaki, H. Huang, C.-R. Du, H. Löwen, and A. V. Ivlev, Buckling of two-dimensional plasma crystals with non-reciprocal interactions, Phys. Rev. E **102**, 043204 (2020).

[72] P. Hartmann, G. J. Kalman, Z. Donkó, and K. Kutasi, Equilibrium properties and phase diagram of two-dimensional Yukawa systems, Phys. Rev. E **72**, 026409 (2005).

[73] R. C. Hibbeler, *Statics and Mechanics of Materials in SI Units* (Pearson, Harlow, 2018).

[74] P. Guyot, A. M. Kraynik, D. Reinelt, and S. Cohen-Addad, Elastic behavior of confined soap froth, Soft Matter **15**, 8227 (2019).

[75] M. L. Falk and J. S. Langer, Dynamics of viscoplastic deformation in amorphous solids, Phys. Rev. E **57**, 7192 (1998).

[76] Z. Fan, E. Ma, and M. L. Falk, Predicting the location of shear band initiation in a metallic glass, Phys. Rev. Mater. **6**, 065602 (2022).

[77] X. Wang, A. Bhattacharjee, and S. Hu, Longitudinal and transverse waves in Yukawa crystals, Phys. Rev. Lett. **86**, 2569 (2001).

[78] See Supplemental Material at http://link.aps.org/supplemental/10.1103/PhysRevResearch.6.033211 for (i) some simulation details, (ii) more results of the orientation dependence of the yield stress under different conditions, and (iii) the evolution of the stress-strain response curves during more forward and backward shear deformation cycles.